Title

Lumped-element axion dark matter detection beyond the magnetoquasistatic limit

Journal

Physical Review D, 108(3)

ISSN

2470-0010

Authors

Benabou, Joshua N

Foster, Joshua W

Kahn, Yonatan

et al.

Publication Date

2023-08-01

DOI

10.1103/physrevd.108.035009

Theory of photoluminescence spectral line shapes of semiconductor nanocrystals

Kailai Lin,[*,†] Dipti Jasrasaria,[†,‖] Jason J. Yoo,[‡] Moungi Bawendi,[‡] Hendrik Utzat,[*,†] and Eran Rabani[*,†,¶,§]

†*Department of Chemistry, University of California, Berkeley, California 94720, USA*
‡*Department of Chemistry, Massachusetts Institute of Technology, Cambridge, Massachusetts 02143, USA*
¶*Materials Sciences Division, Lawrence Berkeley National Laboratory, Berkeley, California 94720, USA*
§*The Raymond and Beverly Sackler Center of Computational Molecular and Materials Science, Tel Aviv University, Tel Aviv 69978, Israel*
‖*Current address: Department of Chemistry, Columbia University, New York, New York 10027, United States*

E-mail: tommy_lin@berkeley.edu; hutzat@berkeley.edu; eran.rabani@berkeley.edu

Abstract

Single-molecule photoluminescence (PL) spectroscopy of semiconductor nanocrystals (NCs) reveals the nature of exciton-phonon interactions in NCs. Understanding the narrow line shapes at low temperatures and the significant broadening as temperature increases remains an open problem. Here, we develop an atomistic model to describe the PL spectrum of NCs, accounting for excitonic effects, phonon dispersion relations, and exciton-phonon couplings. We use single-molecule PL measurements on CdSe/CdS core-shell NCs from $T = 4$ to $T = 290$ K to validate our model and find that the slightly-asymmetric main peak at low temperatures is comprised of a narrow zero-phonon line (ZPL) and several acoustic phonon sidebands. Furthermore, we identify the distinct CdSe optical modes that give rise to the optical phonon sidebands. As the temperature increases, the spectral width shows a stronger dependence on temperature, which we demonstrated to be correlated with frequency shifts and mode-mixing, reflected as higher-order exciton-phonon couplings (Duschinsky rotations). We also model the PL dependence on core size and shell thickness and provide strategies for the design of NCs with narrow linewidths at elevated temperatures.

The optical properties of colloidal semiconductor nanocrystals (NCs) have been extensively studied over the last several decades,[1–7] leading to the development of novel optoelectronic devices.[8–13] Many studies have aimed to understand the photoluminescence (PL) line shapes and, in particular, the dominant channels and couplings governing the homogeneous contributions to the linewidth.[5,14–21] In particular, low-temperature single-NC PL measurements have been commonly used to delineate the homogeneous contributions, indicating complex structures of sidebands resulting from the coupling of excitons to acoustic and optical phonons.[22–28] On the other hand, the exciton-phonon coupling parameters obtained in these low-temperature studies were not able to reconcile the broad, application-relevant, room-temperature emission linewidths, resulting in a lack of consensus on the strength and nature of exciton-phonon interactions in NCs.

A thorough understanding of the structure

of the NC PL spectrum and its temperature dependence calls for an atomistic, parameter-free theoretical approach that calculates the PL line shapes of experimentally relevant NC sizes. For smaller clusters, one can use first-principle methods, but these are limited by computational complexity.[29] Here, we adopt such an approach that accurately describes the exciton fine structure, phonon modes, and exciton-phonon couplings of NCs.[30,31] To test and validate this approach, we compared the predictions from our theory with new, single-NC PL measurements for CdSe/CdS core-shell NCs across a wide range of temperatures, from 4 to 290 K, overcoming common experimental challenges, such as photo-charging, bleaching, and thermal drift.[32] Our model yields results that match very well with the experimental measurements, reconciling the narrow, low-temperature linewidth and weak phonon sidebands with the broad, room-temperature line shape. In addition, we identify the specific phonon modes that lead to the observed phonon sidebands at low temperatures and discuss the contributions of acoustic and surface modes to the "zero-phonon" line across different NC sizes. Furthermore, we discuss the role of dephasing on the spectral line shape and the dependence on temperature.

We start with a model Hamiltonian that describes the ground state, a manifold of excitonic states, a bath of phonons, and the exciton-phonon couplings (expanded to lowest order in the phonon mode coordinates) for an NC,[30] weakly perturbed by an electromagnetic field:

$$\begin{aligned} H = & E_g \left|\psi_g\right\rangle \left\langle\psi_g\right| + \sum_n E_n \left|\psi_n\right\rangle \left\langle\psi_n\right| \\ & + \sum_\alpha \hbar\omega_\alpha b_\alpha^\dagger b_\alpha + \sum_{\alpha nm} V_{n,m}^\alpha \left|\psi_n\right\rangle \left\langle\psi_m\right| q_\alpha \\ & + \varepsilon_0 \sum_n \mu_{gn} \cos(\omega t) \left|\psi_g\right\rangle \left\langle\psi_n\right| + h.c.. \quad (1) \end{aligned}$$

Here, E_g, $|\psi_g\rangle$, E_n, and $|\psi_n\rangle$ are the energies and wavefunctions for the ground and n-th excitonic states, respectively, which are obtained using the atomistic semiempirical pseudopotential method[33–35] combined with the Bethe-Salpeter Equation (BSE).[36,37] We used a Stillinger-Weber force field[38] to describe the equilibrium geometry of the NC and to obtain the normal modes, which have frequencies ω_α and normal mode displacements q_α. The exciton-phonon couplings, $V_{n,m}^\alpha$, between excitonic states $|\psi_m\rangle$ and $|\psi_n\rangle$ through phonon mode α were also calculated from the semiempirical pseudopotential model combined with the BSE.[30] In practice, we only include the diagonal coupling elements, $V_{n,n}^\alpha$, since they dominate the spectral line shape. Finally, the external electromagnetic field with strength ε_0 and frequency ω couples the ground state and the n-th excitonic state through the transition dipole μ_{gn}. More details can be found in the SI and in Ref. 30,39.

The emission spectrum is given by the Fourier transform of the transition dipole autocorrelation function, obtained within linear response theory:[40]

$$\begin{aligned} I(\omega) &= \frac{1}{Q_n} \sum_n e^{-\beta E_n} \int_{-\infty}^{\infty} dt e^{-i\omega t} \left\langle \hat{\mu}_H(t)\, \hat{\mu}_H(0) \right\rangle \\ &= \frac{1}{Q_n} \sum_n e^{-\beta E_n} \left|\mu_{gn}\right|^2 \int_{-\infty}^{\infty} dt e^{i(\omega-\omega_{ng})t} \left\langle F_n(t) \right\rangle , \end{aligned} \quad (2)$$

where we assumed a thermal Boltzmann average over initial excitonic states. In the above equation, $Q_n = \sum_n e^{-\beta E_n}$ is the partition function of excitons and $\omega_{ng} = (E_n - E_g)/\hbar$. The dephasing function, $\langle F_n(t)\rangle$, can be calculated using a cumulant expansion to second order,[41] and is given by the following exact expression for the model Hamiltonian (c.f., Eq. (1)):

$$\left\langle F_n(t) \right\rangle = \exp\left\{ \frac{1}{2\hbar} \sum_\alpha \frac{\left(V_{n,n}^\alpha\right)^2}{\left(\omega_\alpha\right)^3} \left[C_\alpha^{\Re}(t) + i C_\alpha^{\Im}(t) \right] \right\}, \quad (3)$$

where $C_\alpha^{\Re}(t) = \coth(\beta\hbar\omega_\alpha/2)(\cos\omega_\alpha t - 1)$ and $C_\alpha^{\Im}(t) = \sin\omega_\alpha t - \omega_\alpha t$.

In Fig. 1, we plot the PL spectra of a wurtzite 3nm CdSe core / 3 monolayer (ML) CdS shell NC for different temperatures and compare the single NC measurements (green curves) to predictions from our model (solid black curves). In comparing the experimental results with our theoretical predictions, we shifted the onset of emission due to small differences in the optical gaps ($\sim$ 130meV) resulting from an additional 1-2 ML of ZnS coating in the experi-

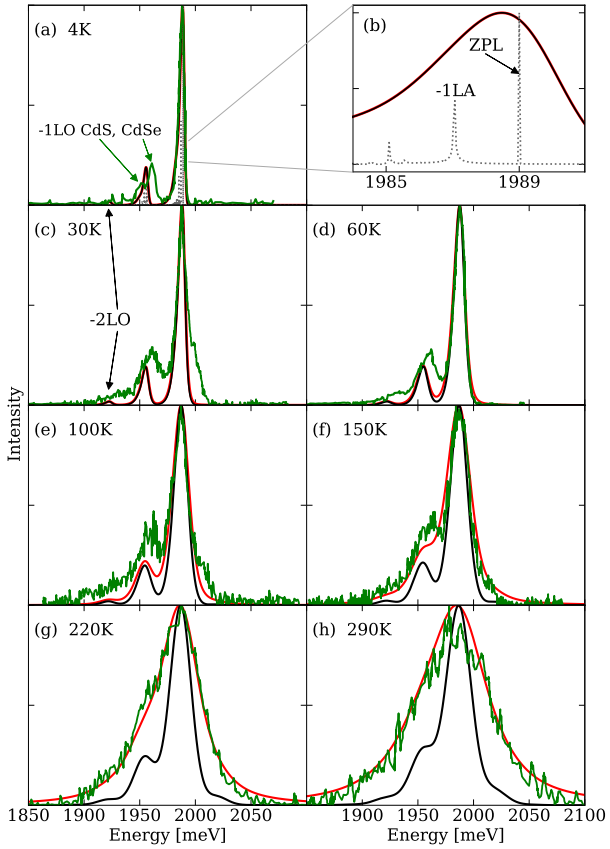

Figure 1: Single-molecule photoluminescence spectra for a 3nm diameter CdSe / 3ML CdS core-shell NC at temperatures ranging from 4 to 290 K. The calculated results from the model Hamiltonian (black curves) and from the empirical inclusion of second-order expansion of exciton-phonon couplings (red curves) are compared to the experimental measurements (green curves). (a) The theoretical model results before (dotted line) and after broadening (black solid line) at 4K are shown. Optical phonon sidebands corresponding to CdSe and CdS are distinguished. (b) A zoomed-in view around the zero-phonon line (ZPL) is shown, identifying several acoustic phonon sidebands. (c) - (h) The calculated and measured PL spectra at 30, 60, 100, 150, 220, and 290K are shown.

ments. Additionally, to compare our simulated results with experiments, we assume a Gaussian broadening of 4meV, which accounts for experimental broadening due to the spectrometer spectral resolution and spectral diffusion. The emission shift and Gaussian broadening are the only empirical parameters used to calculate the line shapes (solid black curves) from Eqs. (2) and (3).

The experimental spectrum at low temperatures consists of a slightly asymmetric narrow center peak and distinct phonon sidebands, which is consistent with earlier studies.[17,21–23,32,42] As the temperature increases, the line shape evolves into a broader structure, and at the crossover temperature $T_c \approx 200$K, turns into a featureless, broad peak. Our theoretical model shows good agreement with the single-NC PL measurements at low and intermediate temperatures ($T \leq T_c$), providing a quantitatively accurate description of the relative positions and intensities of the zero-phonon line (ZPL) and the phonon sidebands, as well as their temperature dependence. As temperature increases above T_c, we observe small deviations between the predicted and measured spectra, which become more significant at higher temperatures, suggesting that there is an additional emission channel that is not included in our model Hamiltonian. One such source for additional broadening is higher-order terms (beyond linear) in the expansions of the exciton-phonon couplings (Duschinsky rotations). The red curves in Fig. 1 include an empirical correction, which is discussed further below, that accounts for the contributions of higher-order couplings at temperatures above T_c, resulting in excellent agreement with the experimental measurements across all temperatures. The crossover temperature is expressed in our model by equating the dephasing rate contributions from linear-order and from higher-order exciton-phonon couplings.

In the limit that $T \to 0$K, the calculated zero-phonon line becomes infinitely narrow with transition energies corresponding to the excitonic (optical) gap,[41,43] as shown in Fig. 1(b). In addition, we observe several *acoustic* phonon sidebands that merge with the broadened ZPL to form one main peak with a slight asymmetry that matches experiments. Our model also identifies some of the *optical* phonon sidebands, particularly those associated with the optical frequency of CdSe (6.29 THz), that remain distinct from the ZPL even at elevated temperatures ($T \leq T_c$). Moreover, due to phonon emission, -2LO phonon satellite over-

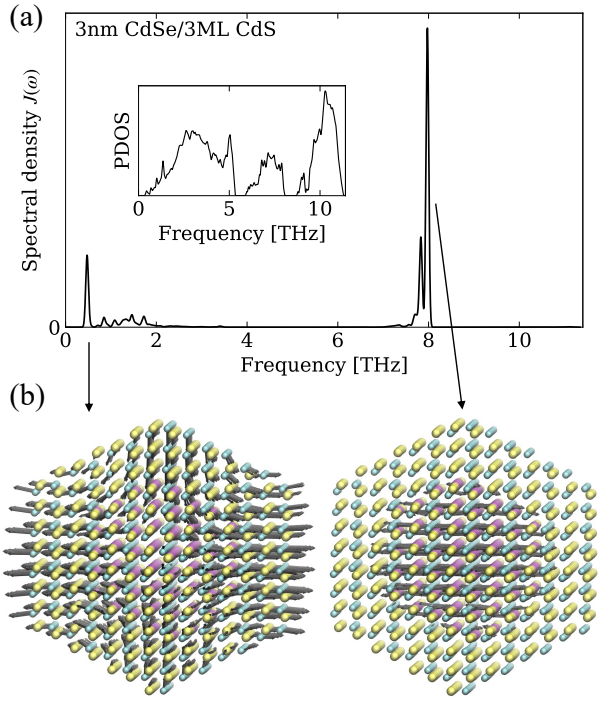

Figure 2: (a) The calculated spectral density of a 3nm core, 3ML shell CdSe/CdS NC using our model. The inset shows the phonon density of states for this core-shell NC. (b) The motions of one acoustic phonon mode and one optical phonon with the strongest coupling to the exciton are shown. Color schemes: blue-Cd, purple-Se, yellow-S, black arrows-phonon mode motion.

tones are visible at energies lower than the optical transition in both the experimental and modeled spectra. The position of the CdSe LO phonon sideband is slightly shifted compared to the experiments, mainly due to inaccuracies of the classical Stillinger-Weber force field, which was parameterized for bulk semiconductors. In addition, the CdS LO phonon sideband observed experimentally at low temperatures (which otherwise merges with the CdSe LO phonon sideband) is absent in the calculated spectra. We cannot exclude emission from the charged trion state experimentally, which is known to be emissive in thick-shell CdSe/CdS, and for which we expect higher coupling to shell LO modes.

To further analyze the contribution of the individual phonon modes to the spectra, we define the spectral density, which measures the strength of couplings between the exciton and the phonon modes:

$$J(\omega) = \sum_{\alpha} \left(\frac{V^{\alpha}_{n,n}}{\omega_{\alpha}} \right)^2 \delta(\omega - \omega_{\alpha}) \qquad (4)$$

The spectral density is plotted in Fig. 2(a) for a 3nm CdSe / 3ML CdS NC. Fig. 2(b) shows an acoustic mode and an optical mode with the strongest coupling to the bright ground state exciton. The motions along the optical mode are primarily restricted to the CdSe core as a result of the localization of the hole to the CdSe core, while the motion along the breathing mode involves atoms in both the core and shell. Similar results were observed for other core sizes and shell thicknesses. The strong coupling to the optical phonons in the core-shell NC is consistent with earlier experimental[17,21,45,46] and theoretical[47–52] investigations.

In Fig. 3, we analyze the temperature dependence of the PL linewidth for single particle and ensemble measurements. At very low temperatures ($k_{\mathrm{B}}T < \hbar\omega_{\mathrm{min}}$), the single particle measurements (green circles) of the full width at half maximum (FWHM) are bound by the experimental resolution ($\approx$ 5meV) and increase monotonically as T increases, with a notable change in the slope at $T_c \approx 200$K. The FWHM for the ensemble measurements from Ref. 44(green squares) is significantly larger than the single particle measurements due to inhomogeneous broadening, with a similar change in the temperature dependence observed at the crossover temperature, which we label as T_c (see further discussion below for the physical interpretation of the crossover temperature).

At low temperatures ($T \leq T_c$), the results obtained from the model Hamiltonian (black curves) show excellent agreement with the experimental measurements at both the single-particle (Fig. 3(a)) and ensemble levels (Fig. 3(b)). At temperatures above T_c, the calculated width (black curves) shows notable deviations from the measured linewidth (green curves), as indicated above. First, we studied the anharmonicity of the atomic motion as a possible source of such deviations by evaluating the finite lifetime of phonons using classical

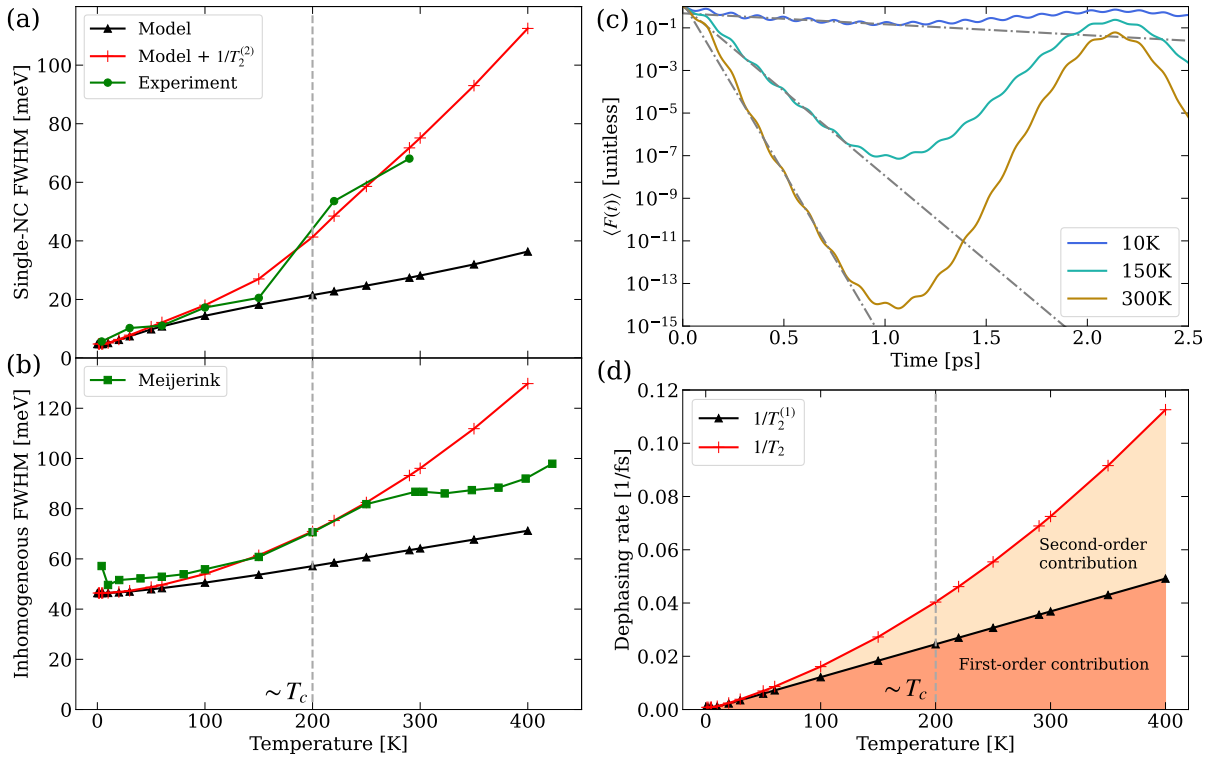

Figure 3: (a) The temperature dependence of PL linewidth of single-NC PL spectra on a 3nm/3ML CdSe/CdS NC. The linewidths calculated by the model (black triangles) are compared to experimental results (green circles). Dephasing contributions from second-order exciton-phonon couplings are included empirically in the red curve. (b) The temperature dependence of inhomogeneous PL linewidth in ensemble measurements on 3nm/2ML CdSe/CdS NCs. Experimental results are shown in green squares and adapted from Ref. 44. The black and red curves show the model results following the same conventions as in panel (a). (c) The dephasing function $\langle F(t)\rangle$ calculated analytically using Eq. (3) in a semi-log plot at three representative temperatures. The first-order dephasing rates (dash-dot lines) are extracted from the exponential-decay regime of the dephasing function before recurrences happen. (d) The dephasing rate contributions from first- and second-order exciton-phonon couplings at various temperatures (see Eq. (5)).

molecular dynamics[53] (see SI for more information). At 300K, incorporating finite phonon lifetimes into the spectrum resulted in an increase of $\approx$ 10meV in the single-NC FWHM, and therefore anharmonic motion is ruled out as the primary mechanism to explain the discrepancy between the experiments and theory. In addition, no temperature-activated spectral diffusion pathways have been identified,[24,32,54] suggesting that role of spectral diffusion at high temperatures is similar to that at low temperatures, where the contribution to the linewidth due to spectral diffusion is negligible.

The discrepancy at high temperatures between the experiments and theory can also result from higher-order expansion terms in the exciton-phonon couplings. To account for these additional decay channels, we empirically correct the long-time decay rate of the dephasing function ($F(t) \propto \exp(-t/T_2)$) as follows:[41]

$$\frac{1}{T_2} = \frac{1}{T_2^{(1)}} + \frac{1}{T_2^{(2)}}\,, \tag{5}$$

where the dephasing rate due to the first-order coupling,

$$\frac{1}{T_2^{(1)}} = \pi \frac{\lambda}{\hbar} \frac{k_B T}{\hbar \omega_c}\,, \tag{6}$$

is extracted from the exponential-decay of the dephasing function (c.f., Eq. (3)), as shown in Fig. 3(c). In the above equation, the reorganization energy is defined as $\lambda = \frac{1}{2}\sum_\alpha \left(\frac{V^\alpha_{n,n}}{\omega_\alpha}\right)^2$.

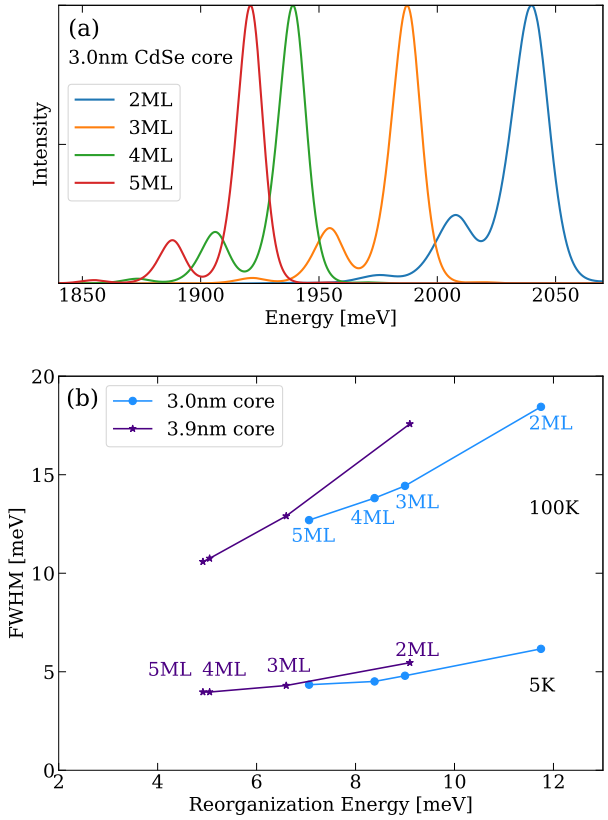

Figure 4: (a) Single-NC PL spectrum progression for a CdSe/CdS core-shell NC of 3 nm core diameter and various shell thicknesses at an intermediate temperature (100K). (b) The spectral linewidth vs. reorganization energy at 5 and 100K for NCs with 3 nm or 3.9 nm diameter CdSe cores and 2 to 5 monolayers (ML) of CdS shells. For all spectra calculations, a Gaussian broadening of 4meV is included to account for the spectrometer spectral resolution in the experiments.

ω_c is the characteristic frequency of the bath. Assuming that the second-order coupling terms dominate the contribution from higher-order terms, the temperature dependence can be approximated by:[41]

$$\frac{1}{T_2^{(2)}} = W^2\pi \int_0^\infty d\omega n(\omega)(n(\omega)+1)\omega^2 J^2(\omega)\,, \tag{7}$$

where W is the magnitude of second-order exciton-phonon coupling and is determined empirically. $n(\omega)$ is the Bose-Einstein distribution, and $J(\omega)$ is the spectral density defined in Eq. (4). In Fig. 3(d), we plot the total (red curve, Eq. 5) and first-order (black curve) dephasing rates as a function of temperatures. At low temperatures, the dephasing rate is governed by the first-order term, while as the temperature increases, the contributions of the first- and higher-order terms become comparable. The temperature dependence of the total dephasing rate explains the change in slope of the FWHM as temperature increases above T_c, as shown by the red curves in Fig. 3(a) and (b). At temperatures around $k_B T_c = 2/W^2\lambda$, the first-order and second-order dephasing rates contribute equally, leading to a temperature-crossover behavior.

Upon validating our model Hamiltonian against single-NC and ensemble PL measurements below T_c, we applied the model to a series of CdSe/CdS core-shell nanocrystals of various core sizes and shell thicknesses at an intermediate temperature of 100K, at which distinct phonon sidebands are visible, as shown in Fig. 4. The intermediate-temperature spectra are calculated with a Gaussian broadening of 4meV that accounts for the spectrometer spectral resolution in the experiments. We observe that for the same core size and for increasing shell thickness, the energy of the optical transition decreases, as expected due to quantum confinement effects. In addition, the reorganization energy, which is a measure of the strength of exciton-phonon couplings, also decreases with increasing shell thickness and increasing core size.[30,39] As a result, the widths of both the ZPL and the LO phonon sideband decrease for larger-core and thicker-shell NCs, but the effect is somewhat more pronounced for the ZPL.

Panel (b) of Fig. 4 shows the dependence of the zero-phonon linewidth on the shell thickness and the reorganization energy, respectively. The reorganization energy correlates with measured Stokes shifts,[31,55] and thus, can also be inferred from experiments. At 100K, the zero-phonon linewidth decreases by $\approx$ 6meV as the shell thickness increases from 2 to 5 monolayers for both core sizes and seems to saturate beyond $\approx 5-6$ monolayers for the larger core. At 5K, the ZPL linewidth also shows a similar linear dependence on the re-

organization energy, with a less steep slope and smaller change in FWHM ($2-3$meV as the shell thickness increases). Given that the first-order exciton-phonon coupling dominates the dephasing rate $1/T_2$ below $T_c \approx 200$K, the near-linear dependence of the FWHM on the reorganization energy at 100K and 5K can be explained by Eq. (6) where the first-order dephasing rate depends linearly on reorganization energy.

In this work, we developed an approach to calculate the photoluminescence spectra of CdSe/CdS core-shell nanocrystals and compared our prediction with single-molecule PL measurements for a wide range of temperatures, overcoming challenges of blinking and rapid charging-induced spectral shifts. Our approach utilizes an atomistic force field to model the phonon modes, and the semiempirical pseudopotential model combined with the Bethe-Salpeter Equation to describe the excitonic structure and the exciton-phonon couplings to lowest order in the phonon modes in NCs.

The single-NC experiments reveal low-temperature spectra of a narrow main peak accompanied by distinct phonon sidebands and broad, featureless room-temperature spectra. Using linear response theory, we showed that the calculated results accurately reproduce our measured PL spectra below a crossover temperature, $T_c \sim 200\,\mathrm{K}$. In the low-temperature regime, our model explains the nature of the narrow, slightly-asymmetric zero-phonon line. By analyzing the coupling of individual phonon modes to the ground state bright exciton, we identified the specific acoustic and optical phonon modes that lead to the sidebands.

As temperature increases above T_c, the measured zero-phonon linewidth increases more rapidly with temperature. Anharmonic atomic motion is examined and ruled out as the source of further broadening in PL linewidth. We attributed this crossover behavior to the increasing significance of higher-order exciton-phonon coupling, which is not included in our model, and showed that including a second-order coupling term with a single parameter accounts for the behavior of the spectral linewidth above T_c.

We applied our model to predict the behavior of the PL spectra for CdSe/CdS NCs of different core sizes and shell thicknesses and found that NCs with larger cores and thicker shells have smaller overall exciton-phonon coupling, as demonstrated by their reorganization energies, as well as narrower ZPL and phonon sidebands. The theoretical approach established in this work assists future designs of novel semiconductor nanocrystal materials. Increasing core size, increasing shell thickness, reducing exciton-acoustic-phonon coupling, and reducing second-order exciton-phonon coupling (Duschinsky rotations) have all been demonstrated as viable paths to achieve narrow room-temperature linewidth in relevant NC-based technologies.

Acknowledgement E.R. acknowledges support from the U.S. Department of Energy, Office of Science, Office of Basic Energy Sciences, Materials Sciences and Engineering Division, under Contract No. DE-AC02-05-CH11231 within the Fundamentals of Semiconductor Nanowire Program (KCPY23). Methods used in this work were provided by the Center for Computational Study of Excited State Phenomena in Energy Materials (C2SEPEM), which is funded by the U.S. Department of Energy, Office of Science, Basic Energy Sciences, Materials Sciences and Engineering Division, via contract no. DE-AC02- 05CH11231, as part of the Computational Materials Sciences Program. Computational resources were provided in part by the National Energy Research Scientific Computing Center (NERSC), a U.S. Department of Energy Office of Science User Facility operated under contract no. DE-AC02-05CH11231. D.J. acknowledges the support of the Computational Science Graduate Fellowship from the U.S. Department of Energy under grant no. DE-SC0019323.

Supporting Information Available

Further details are provided on nanocrystal synthesis, single-nanocrystal spectroscopy, theoretical methods for parametrizing the

nanocrystal model hamiltonian, the linear response model for vibronic spectrum, and anharmonicity. See xxx [link].

References

(1) Bawendi, M. G.; Steigerwald, M. L.; Brus, L. E. The Quantum Mechanics of Larger Semiconductor Clusters ("Quantum Dots"). *Annual Review of Physical Chemistry* **1990**, *41*, 477–496.

(2) Brus, L. Quantum crystallites and nonlinear optics. *Applied Physics A* **1991**, *53*, 465–474.

(3) Alivisatos, A. P. Perspectives on the Physical Chemistry of Semiconductor Nanocrystals. *The Journal of Physical Chemistry* **1996**, *100*, 13226–13239.

(4) Efros, A. L.; Rosen, M. The eletronic structure of semiconductor nanocrystals. *Annual Review of Materials Science* **2000**, *30*, 475.

(5) Gómez, D. E.; Califano, M.; Mulvaney, P. Optical properties of single semiconductor nanocrystals. *Physical Chemistry Chemical Physics* **2006**, *8*, 4989–5011.

(6) Klimov, V. I. Spectral and Dynamical Properties of Multiexcitons in Semiconductor Nanocrystals. *Annual Review of Physical Chemistry* **2007**, *58*, 635–673.

(7) Efros, A. L.; Brus, L. E. Nanocrystal Quantum Dots: From Discovery to Modern Development. *ACS Nano* **2021**, *15*, 6192–6210.

(8) Somers, R. C.; Bawendi, M. G.; Nocera, D. G. CdSe nanocrystal based chem-/bio- sensors. *Chemical Society Reviews* **2007**, *36*, 579–591.

(9) García-Santamaría, F.; Chen, Y.; Vela, J.; Schaller, R. D.; Hollingsworth, J. A.; Klimov, V. I. Suppressed auger recombination in "Giant" nanocrystals boosts optical gain performance. *Nano Letters* **2009**, *9*, 3482–3488.

(10) Wood, V.; Bulović, V. Colloidal quantum dot light-emitting devices. *Nano Reviews* **2010**, *1*, 5202.

(11) Ledentsov, N. N. Quantum Dot Laser. *Semicond. Sci. Technol.* **2011**, *26*, 14001.

(12) Bronstein, N. D.; Yao, Y.; Xu, L.; O'Brien, E.; Powers, A. S.; Ferry, V. E.; Alivisatos, A. P.; Nuzzo, R. G. Quantum Dot Luminescent Concentrator Cavity Exhibiting 30-fold Concentration. *ACS Photonics* **2015**, *2*, 1576.

(13) Owen, J.; Brus, L. Chemical Synthesis and Luminescence Applications of Colloidal Semiconductor Quantum Dots. *Journal of the American Chemical Society* **2017**, *139*, 10939–10943.

(14) Bawendi, M. G.; Wilson, W. L.; Rothberg, L.; Carroll, P. J.; Jedju, T. M.; Steigerwald, M. L.; Brus, L. E. Electronic structure and photoexcited-carrier dynamics in nanometer-size CdSe clusters. *Physical Review Letters* **1990**, *65*, 1623–1626.

(15) Empedocles, S. A.; Norris, D. J.; Bawendi, M. G. Photoluminescence Spectroscopy of Single CdSe Nanocrystallite Quantum Dots. *Physical Review Letters* **1996**, *77*, 3873–3876.

(16) Heitz, R.; Mukhametzhanov, I.; Stier, O.; Madhukar, A.; Bimberg, D. Enhanced Polar Exciton-LO-Phonon Interaction in Quantum Dots. *Phys. Rev. Lett.* **1999**, *83*, 4654.

(17) Salvador, M. R.; Graham, M. W.; Scholes, G. D. Exciton-Phonon Coupling and Disorder in the Excited States of CdSe Colloidal Quantum Dots. *J. Chem. Phys.* **2006**, *125*, 184709.

(18) Morello, G.; De Giorgi, M.; Kudera, S.; Manna, L.; Cingolani, R.; Anni, M. Temperature and Size Dependence of Nonradiative Relaxation and Exciton-Phonon Coupling in Colloidal CdTe Quantum Dots. *J. Phys. Chem. C* **2007**, *111*, 5846.

(19) Sagar, D. M.; Cooney, R. R.; Sewall, S. L.; Dias, E. A.; Barsan, M. M.; Butler, I. S.; Kambhampati, P. Size Dependent, State-Resolved Studies of Exciton-Phonon Couplings in Strongly Confined Semiconductor Quantum Dots. *Phys. Rev. B: Condens. Matter Mater. Phys.* **2008**, *77*, 1.

(20) Sagar, D. M.; Cooney, R. R.; Sewall, S. L.; Kambhampati, P. State-Resolved Exciton-Phonon Couplings in CdSe Semiconductor Quantum Dots. *J. Phys. Chem. C* **2008**, *112*, 9124.

(21) Lin, C.; Gong, K.; Kelley, D. F.; Kelley, A. M. Size-Dependent Exciton-Phonon Coupling in CdSe Nanocrystals through Resonance Raman Excitation Profile Analysis. *J. Phys. Chem. C* **2015**, *119*, 7491.

(22) Besombes, L.; Kheng, K.; Marsal, L.; Mariette, H. Acoustic phonon broadening mechanism in single quantum dot emission. *Physical Review B* **2001**, *63*, 155307.

(23) Htoon, H.; Cox, P. J.; Klimov, V. I. Structure of Excited-State Transitions of Individual Semiconductor Nanocrystals Probed by Photoluminescence Excitation Spectroscopy. *Physical Review Letters* **2004**, *93*, 187402.

(24) Coolen, L.; Brokmann, X.; Spinicelli, P.; Hermier, J.-P. Emission Characterization of a Single CdSe-ZnS Nanocrystal with High Temporal and Spectral Resolution by Photon-Correlation Fourier Spectroscopy. *Physical Review Letters* **2008**, *100*, 27403.

(25) Fernée, M. J.; Littleton, B. N.; Cooper, S.; Rubinsztein-Dunlop, H.; Gómez, D. E.; Mulvaney, P. Acoustic Phonon Contributions to the Emission Spectrum of Single CdSe Nanocrystals. *The Journal of Physical Chemistry C* **2008**, *112*, 1878–1884.

(26) Fernée, M. J.; Tamarat, P.; Lounis, B. Cryogenic Single-Nanocrystal Spectroscopy: Reading the Spectral Fingerprint of Individual CdSe Quantum Dots. *The Journal of Physical Chemistry Letters* **2013**, *4*, 609–618.

(27) Cui, J.; Beyler, A. P.; Marshall, L. F.; Chen, O.; Harris, D. K.; Wanger, D. D.; Brokmann, X.; Bawendi, M. G. Direct probe of spectral inhomogeneity reveals synthetic tunability of single-nanocrystal spectral linewidths. *Nature Chemistry* **2013**, *5*, 602–606.

(28) Cui, J.; Beyler, A. P.; Coropceanu, I.; Cleary, L.; Avila, T. R.; Chen, Y.; Cordero, J. M.; Heathcote, S. L.; Harris, D. K.; Chen, O.; Cao, J.; Bawendi, M. G. Evolution of the Single-Nanocrystal Photoluminescence Linewidth with Size and Shell: Implications for Exciton-Phonon Coupling and the Optimization of Spectral Linewidths. *Nano Letters* **2016**, *16*, 289–296.

(29) Palato, S.; Seiler, H.; Nijjar, P.; Prezhdo, O.; Kambhampati, P. Atomic Fluctuations in Electronic Materials Revealed by Dephasing. *Proc. Natl. Acad. Sci. U. S. A.* **2020**, *117*, 11940.

(30) Jasrasaria, D.; Rabani, E. Interplay of Surface and Interior Modes in Exciton-Phonon Coupling at the Nanoscale. *Nano Letters* **2021**, *21*, 8741–8748.

(31) Jasrasaria, D.; Weinberg, D.; Philbin, J. P.; Rabani, E. Simulations of nonradiative processes in semiconductor nanocrystals. *The Journal of Chemical Physics* **2022**, *157*, 20901.

(32) Empedocles, S. A.; Bawendi, M. G. Influence of Spectral Diffusion on the Line Shapes of Single CdSe Nanocrystallite Quantum Dots. *The Journal of Physical Chemistry B* **1999**, *103*, 1826–1830.

(33) Wang, L. W.; Zunger, A. Local-density-derived semiempirical pseudopotentials. *Physical Review B* **1995**, *51*, 17398.

(34) Wang, L. W.; Zunger, A. Pseudopotential Calculations of Nanoscale CdSe Quantum Dots. *Phys. Rev. B: Condens. Matter Mater. Phys.* **1996**, *53*, 9579.

(35) Rabani, E.; Hetényi, B.; Berne, B. J.; Brus, L. E. Electronic Properties of CdSe Nanocrystals in the Absence and Presence of a Dielectric Medium. *J. Chem. Phys.* **1999**, *110*, 5355.

(36) Rohlfing, M.; Louie, S. G. Electron-hole excitations and optical spectra from first principles. *Physical Review B* **2000**, *62*, 4927–4944.

(37) Eshet, H.; Grünwald, M.; Rabani, E. The Electronic Structure of CdSe/CdS Core/Shell Seeded Nanorods: Type-I or Quasi-Type-II? *Nano Letters* **2013**, *13*, 5880–5885.

(38) Zhou, X. W.; Ward, D. K.; Martin, J. E.; Van Swol, F. B.; Cruz-Campa, J. L.; Zubia, D. Stillinger-Weber Potential for the II-VI Elements Zn-Cd-Hg-S-Se-Te. *Phys. Rev. B: Condens. Matter Mater. Phys.* **2013**, *88*, 85309.

(39) Jasrasaria, D.; Rabani, E. Correction to Interplay of Surface and Interior Modes in Exciton–Phonon Coupling at the Nanoscale. *Nano Letters* **2022**, *2021*, 8741–8748.

(40) Mukamel, S. *Principles of Nonlinear Optical Spectroscopy*; Oxford series in optical and imaging sciences; Oxford University Press, 1995.

(41) Skinner, J. L.; Hsu, D. Pure dephasing of a two-level system. *Journal of Physical Chemistry* **1986**, *90*, 4931–4938.

(42) Nomura, S.; Kobayashi, T. Exciton–LO-Phonon Couplings in Spherical Semiconductor Microcrystallites. *Phys. Rev. B: Condens. Matter Mater. Phys.* **1992**, *45*, 1305.

(43) Coalson, R. D. A spin-boson model for spectroscopy involving nonadiabatically coupled potential energy surfaces ARTICLES YOU MAY BE INTERESTED IN. *J. Chem. Phys* **1987**, *86*, 995.

(44) Van Der Bok, J. C.; Dekker, D. M.; Peerlings, M. L.; Salzmann, B. B.; Meijerink, A. Luminescence Line Broadening of CdSe Nanoplatelets and Quantum Dots for Application in w-LEDs. *Journal of Physical Chemistry C* **2020**, *124*, 12153–12160.

(45) Scamarcio, G.; Spagnolo, V.; Ventruti, G.; Lugará, M.; Righini, G. Size Dependence of Electron–LO-Phonon Coupling in Semiconductor Nanocrystals. *Phys. Rev. B: Condens. Matter Mater. Phys.* **1996**, *53*, R10489.

(46) Lin, C.; Gong, K.; Kelley, D. F.; Kelley, A. M. Electron-Phonon Coupling in CdSe/CdS Core/Shell Quantum Dots. *ACS Nano* **2015**, *9*, 8131.

(47) Klein, M. C.; Hache, F.; Ricard, D.; Flytzanis, C. Size Dependence of Electron-Phonon Coupling in Semiconductor Nanospheres: The Case of CdSe. *Phys. Rev. B: Condens. Matter Mater. Phys.* **1990**, *42*, 11123.

(48) Takagahara, T. Electron-Phonon Interactions in Semiconductor Nanocrystals. *J. Lumin.* **1996**, *70*, 129.

(49) Hamma, M.; Miranda, R. P.; Vasilevskiy, M. I.; Zorkani, I. Calculation of the Huang-Rhys Parameter in Spherical Quantum Dots: The Optical Deformation Potential Effect. *J. Phys.: Condens. Matter* **2007**, *19*, 346215.

(50) Kelley, A. M. Electron-phonon coupling in cdse nanocrystals from an atomistic phonon model. *ACS Nano* **2011**, *5*, 5254–5262.

(51) Han, P.; Bester, G. First-Principles Calculation of the Electron-Phonon Interaction in Semiconductor Nanoclusters. *Phys. Rev. B: Condens. Matter Mater. Phys.* **2012**, *85*, 235422.

(52) Han, P.; Bester, G. Fundamental Difference Between Measured and Calculated Exciton-Phonon Coupling in Nanostructures. *Phys. Rev. B: Condens. Matter Mater. Phys.* **2019**, *99*, 100302.

(53) Guzelturk, B. et al. Dynamic lattice distortions driven by surface trapping in semiconductor nanocrystals. *Nature Communications 2021 12:1* **2021**, *12*, 1–9.

(54) Empedocles, S. A.; Bawendi, M. G. Quantum-Confined Stark Effect in Single CdSe Nanocrystallite Quantum Dots. *Science* **1997**, *278*, 2114–2117.

(55) Liptay, T. J.; Marshall, L. F.; Rao, P. S.; Ram, R. J.; Bawendi, M. G. Anomalous Stokes Shift in CdSe Nanocrystals. *Phys. Rev. B: Condens. Matter Mater. Phys.* **2007**, *76*, 1.

Graphical TOC Entry